



Oceanic mass transport by mesoscale eddies

Zhengguang Zhang *et al.*
Science **345**, 322 (2014);
DOI: 10.1126/science.1252418

This copy is for your personal, non-commercial use only.

If you wish to distribute this article to others, you can order high-quality copies for your colleagues, clients, or customers by [clicking here](#).

Permission to republish or repurpose articles or portions of articles can be obtained by following the guidelines [here](#).

The following resources related to this article are available online at www.sciencemag.org (this information is current as of August 1, 2014):

Updated information and services, including high-resolution figures, can be found in the online version of this article at:

<http://www.sciencemag.org/content/345/6194/322.full.html>

Supporting Online Material can be found at:

<http://www.sciencemag.org/content/suppl/2014/06/25/science.1252418.DC1.html>

This article **cites 22 articles**, 4 of which can be accessed free:

<http://www.sciencemag.org/content/345/6194/322.full.html#ref-list-1>

This article appears in the following **subject collections**:

Oceanography

<http://www.sciencemag.org/cgi/collection/oceans>

- R. D. Muench, J. E. Overland, Eds. (Geophysical Monograph Series, American Geophysical Union, Washington, DC, 1994), vol. 85, pp. 295–311.
5. P. U. Clark, D. Pollard, *Paleoceanography* **13**, 1–9 (1998).
 6. L. Lisiecki, M. E. Raymo, *Paleoceanography* **20**, PA1003 (2005).
 7. P. U. Clark *et al.*, *Quat. Sci. Rev.* **25**, 3150–3184 (2006).
 8. H. Elderfield *et al.*, *Science* **337**, 704–709 (2012).
 9. W. S. Broecker, *Oceanography* **4**, 79–89 (1991).
 10. M. E. Raymo, W. F. Ruddiman, N. J. Shackleton, D. W. Oppo, *Earth Planet. Sci. Lett.* **97**, 353–368 (1990).
 11. E. L. McClymont, S. M. Sostdian, A. Rosell-Melé, Y. Rosenthal, *Earth Sci. Rev.* **123**, 173–193 (2013).
 12. M. E. Raymo, *Paleoceanography* **12**, 577–585 (1997).
 13. P. Huybers, *Quat. Sci. Rev.* **26**, 37–55 (2007).
 14. H. Gildor, E. Tziperman, *Paleoceanography* **15**, 605–615 (2000).
 15. A. Martínez-García, A. Rosell-Melé, E. L. McClymont, R. Gersonde, G. H. Haug, *Science* **328**, 1550–1553 (2010).
 16. B. Hönisch, N. G. Hemming, D. Archer, M. Siddall, J. F. McManus, *Science* **324**, 1551–1554 (2009).
 17. J. R. Toggweiler, *Paleoceanography* **14**, 571–588 (1999).
 18. J. Schmitt *et al.*, *Science* **336**, 711–714 (2012).
 19. P. Köhler, R. Bintanja, *Clim. Past* **4**, 311–332 (2008).
 20. P. Köhler, H. Fischer, J. Schmitt, *Paleoceanography* **25**, PA1213 (2010).
 21. D. A. Hodell, K. A. Venz, C. D. Charles, U. S. Ninnemann, *Geochem. Geophys. Geosyst.* **4**, 1–19 (2003).
 22. K. Tachikawa, C. Jeandel, M. Roy-Barman, *Earth Planet. Sci. Lett.* **170**, 433–446 (1999).
 23. S. L. Goldstein, S. R. Hemming, “Long-lived isotopic tracers in oceanography, paleoceanography and ice sheet dynamics,” in *Treatise on Geochemistry* (Elsevier, New York, 2003), vol. 6, pp. 453–498.
 24. A. M. Piotrowski, S. L. Goldstein, S. R. Hemming, R. G. Fairbanks, *Science* **307**, 1933–1938 (2005).
 25. W. Abouchami, S. L. Goldstein, S. J. G. Gazer, A. Eisenhauer, A. Mangini, *Geochim. Cosmochim. Acta* **61**, 3957–3974 (1997).
 26. K. W. Burton, D.-C. Lee, J. N. Christensen, A. N. Halliday, J. R. Hein, *Earth Planet. Sci. Lett.* **171**, 149–156 (1999).
 27. H.-F. Ling *et al.*, *Earth Planet. Sci. Lett.* **232**, 345–361 (2005).
 28. K. A. Venz, D. A. Hodell, *Palaeogeogr. Palaeoclimatol. Palaeoecol.* **182**, 197–220 (2002).
 29. T. Stichel, M. Frank, J. Rickli, B. A. Haley, *Earth Planet. Sci. Lett.* **317–318**, 282–294 (2012).
 30. W. B. Curry, D. W. Oppo, *Paleoceanography* **20**, PA1017 (2005).
 31. A. Ganachaud, C. Wunsch, *Nature* **408**, 453–457 (2000).
 32. R. Bintanja, R. S. W. van de Wal, *Nature* **454**, 869–872 (2008).
 33. W. S. Broecker, E. Maier-Reimer, *Global Biogeochem. Cycles* **6**, 315–320 (1992).
 34. A. Mackensen, H. W. Hubberten, T. Bickert, G. Fischer, D. K. Fütterer, *Paleoceanography* **8**, 587–610 (1993).
 35. D. Lüthi *et al.*, *Nature* **453**, 379–382 (2008).
 36. L. E. Lisiecki, *Geophys. Res. Lett.* **37**, L21708 (2010).

ACKNOWLEDGMENTS

We acknowledge support from NSF grant OCE-10-31198. We also thank two anonymous reviewers for valuable comments. This study was partly supported by the Storke Endowment of the Department of Earth and Environmental Sciences, Columbia University. Samples were provided by the ODP, which is sponsored by the NSF and participating countries under management of Joint Oceanographic Institutions. R. Lupien helped with sample processing. The data in this paper will be available in the supplementary materials and deposited with National Oceanic and Atmospheric Administration–National Climate Data Center at www.ncdc.noaa.gov. This is LDEO contribution number 7809.

SUPPLEMENTARY MATERIALS

www.sciencemag.org/content/345/6194/318/suppl/DC1
Materials and Methods
Supplementary Text
Figs. S1 to S3
Tables S1 and S2
References (37–50)

16 December 2013; accepted 16 June 2014
Published online 26 June 2014;
10.1126/science.1249770

OCEANOGRAPHY

Oceanic mass transport by mesoscale eddies

Zhengguang Zhang,¹ Wei Wang,^{1*} Bo Qiu²

Oceanic transports of heat, salt, fresh water, dissolved CO₂, and other tracers regulate global climate change and the distribution of natural marine resources. The time-mean ocean circulation transports fluid as a conveyor belt, but fluid parcels can also be trapped and transported discretely by migrating mesoscale eddies. By combining available satellite altimetry and Argo profiling float data, we showed that the eddy-induced zonal mass transport can reach a total meridionally integrated value of up to 30 to 40 sverdrups (Sv) (1 Sv = 10⁶ cubic meters per second), and it occurs mainly in subtropical regions, where the background flows are weak. This transport is comparable in magnitude to that of the large-scale wind- and thermohaline-driven circulation.

Heat and material transports in oceans play a dominant role in regulating Earth's climate and in controlling the oceanic absorption of greenhouse gases that are responsible for global warming. Large-scale wind- and thermohaline-driven ocean circulation has traditionally been regarded to constitute the major part of the oceanic transport, and its spatiotemporal variations to have profound climate and biogeochemical impacts. However, by tracking water masses (1) and radiocarbons (2), observational studies have revealed that the large-scale circulation alone cannot explain the oceanic transports. Since the detection of their ubiquitous presence in the oceans more than three decades ago, oceanic mesoscale eddies with length scales about 50 to 300 km have been recognized as key contributors in transporting heat, dissolved carbon, and other biogeochemical tracers (3–6).

Unlike the large-scale circulation that transports fluids and their properties continuously, mesoscale eddies can trap fluid parcels within the eddy core and transport them discretely (7, 8). Our theoretical understanding of the processes involving mesoscale eddies remains, however, incomplete. For example, many existing studies have treated transport by eddies as a simple diffusion process that tends to obscure the redistribution processes of dynamical and biogeochemical tracers (9). In addition to the theoretical understanding, it is equally important to quantify the eddy-induced fluid volume transport on the basis of available observational data. There exist, however, two major challenges for such quantification: First, there is no widely accepted criterion that defines the volume of fluid trapped by an eddy; and, second, accurate vertical structures of the mesoscale eddies are often observationally inaccessible.

In defining the fluid trapped by eddies, all existing criteria are kinematic in nature; they are

inherently descriptive and depend on the choice of reference frame (6–8, 10). From a dynamical point of view, the movement of a rotating fluid can be depicted by a dynamically conserved quantity: potential vorticity (PV), its tendency to spin. PV contours have long been used to identify the trajectory of fluid particles in the ocean (11), and fluid tends to be trapped within the closed PV contours (12). A classical demonstration of this constraint is the Taylor Column in the homogeneous-fluid rotating tank experiment (13). For an adiabatic stratified ocean, fluid motion is constrained on isopycnal surfaces. If a PV contour on an isopycnal is closed because of eddy perturbations, the fluid trapped inside this closed contour will move with the eddy. In the present work, the outmost closed PV contours on isopycnals were used as the criterion to determine the boundary of fluid trapped by eddies.

Regarding the second challenge of capturing the three-dimensional (3D) structures of mesoscale eddies, our recent study has demonstrated that they can be reconstructed by combining the high-resolution satellite altimeter data and concurrent Argo profiling float temperature/salinity data (14). Once the 3D potential density (called density hereafter) field is reconstructed from the altimeter sea surface height (SSH) measurements, we are able to evaluate the eddy-perturbed PV field and finally quantify the fluid volume trapped by the moving eddies (15). To verify our method of reconstructing the eddy density field, we used independent mooring observations from different regions of the world oceans: the Labrador Sea, the Arabian Sea, and the Kuroshio Extension (Fig. 1). The reconstructed eddy density structures are found to compare favorably with the mooring results for both the warm- and cold-core eddies. The relative errors of the reconstructed isopycnal surface displacement are estimated to be 20% of the variance (15), an uncertainty level that is acceptable for estimating the fluid volume trapped by mesoscale eddies.

For illustration, three isopycnal surfaces of an observed warm-core eddy in the subtropical North Pacific are presented in Fig. 2A. The isopycnal surfaces of this warm-core eddy exhibit a concave

¹Physical Oceanography Lab, Qingdao Collaborative Innovation Center of Marine Science and Technology, Ocean University of China, Qingdao, People's Republic of China.
²Department of Oceanography, University of Hawaii at Manoa, Honolulu, HI, USA.

*Corresponding author. E-mail: wei@ouc.edu.cn

shape. The upper isopycnal surface outcrops at the sea surface and envelops a bulk of warm water. All PV contours on this isopycnal are closed, and the boundary of the trapped water coincides with the outcrop line. On the middle isopycnal of the eddy (at ~ 500 m depth), the PV contours near the eddy core are closed, whereas those outside the eddy core are open; in this case, the eddy traps only the fluid within the outermost closed PV contour. As the eddy perturbation decays with depth, the area enclosed by the closed PV contours diminishes on denser isopycnals,

and the eddy loses its ability to trap water in these deep layers. The outermost closed PV contour on each isopycnal forms a 3D conic surface (the transparent black surface in Fig. 2A), and it is this surface that delineates the boundary of the fluid trapped by this warm-core eddy. For comparison, a cold-core eddy detected in the same geographical region is presented in Fig. 2B, and the fluid trapped by this cold-core eddy exhibits a somewhat different vertical enveloping shape.

From the sequential SSH maps from the satellite altimeter measurements, we evaluated the

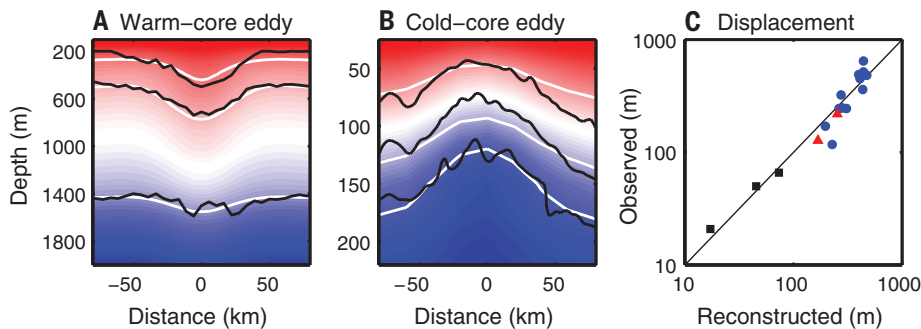


Fig. 1. Comparison between observed and reconstructed eddy density fields. (A) Potential density section across a warm-core eddy at 60.6°N , 52.4°W in the Labrador Sea on 11 October 2008. The horizontal ordinate is the distance to the eddy center, and the vertical ordinate is depth. Colored shades denote the reconstructed density field, with white curves representing the isopycnals at 2765 kg m^{-3} , 2770 kg m^{-3} , and 2775 kg m^{-3} . The corresponding isopycnal surfaces from the mooring observations are indicated by black curves (25). (B) Potential density section across a cold-core eddy at 15.5°N , 61.5°E in the Arabian Sea on 30 November 1994. White and black contours denote the isopycnals at 24.5 kg m^{-3} , 25.5 kg m^{-3} , and 26.0 kg m^{-3} . (C) Comparison of the reconstructed displacement with the observations at the eddy centers. Blue circles represent the 277 kg m^{-3} isopycnal displacement of 12 eddies observed in the Labrador Sea. Black squares represent the 26.0 kg m^{-3} isopycnal displacement of three eddies observed in the Arabian Sea. Red triangles represent the 27.4 kg m^{-3} isopycnal displacement of two eddies observed in the Kuroshio Extension (15).

propagation speed of individual eddies by adopting a Lagrangian tracking method (16, 17). With the eddy propagation speed and its volume of trapped fluid at hand, the eddy-induced mass transport is readily quantifiable (15). Figure 3A shows the global distribution of the eddy-induced zonal transport based on the altimeter SSH data of 1992–2010. A remarkable feature is that the regions of large westward eddy transport are located in all latitude bands between 20° to 40° . Also noteworthy is that an enhanced eddy-induced eastward transport occurs along the Antarctic Circumpolar Current path south of 40°S . When integrated over the entire latitude range from 80°S to 80°N , the total zonal eddy-induced transports add up to 30 to 40 Sv westward and 5 to 10 Sv eastward (Fig. 3B). The global distribution of eddy-induced meridional transport is shown in Fig. 4A. Geographically, the meridional eddy transport has a poleward tendency within the tropical regions (20°S to 20°N) and an equatorward tendency in the subtropical regions (20°N to 60°N and 20°S to 60°S). This meridional eddy transport in many parts of the world oceans moves in the same direction as the meridional wind-forced Ekman transport. The convergent latitudes for the meridional eddy transport, however, appear equatorward of the convergent latitudes for the meridional Ekman transport. Because of the predominance of westward propagations by the mesoscale eddies (17), the zonally integrated eddy-induced meridional transport is on the order of several sverdrups, which is much smaller than the zonal eddy-induced mass transport (Fig. 4B). The relative errors in these transport values are estimated at about 20% (15).

As a comparison, the transports of the wind-driven gyres in the Pacific, Atlantic, and Indian Oceans are 20 to 60 Sv, 20 to 50 Sv, and 10 to 25 Sv, respectively, and the transports of the thermohaline circulation in these three oceans are 10 to 20 Sv, 9 to 20 Sv, and 10 to 15 Sv, respectively (18, 19). The 30- to 40-Sv value of the eddy-induced zonal transport is comparable in magnitude with the large-scale wind- and thermohaline-driven circulation. Apart from the Southern Ocean, these zonal transports work to accumulate water onto the western side of the ocean basins, implying that the mesoscale eddies can exert a strong impact on the transports of the western boundary currents. Indeed, observations of the Kuroshio transport east of Taiwan reveal that its interannual variation has no obvious correlation with the large-scale wind fluctuations but exhibits a good correspondence with the eddy kinetic energy level east of the island of Taiwan (20). As indicated in Fig. 3A, the region east of Taiwan is the strongest hot spot of eddy-induced transport in the North Pacific Ocean. With the amount of mesoscale eddies modulating on the interannual and decadal time scales (21), the eddy-induced zonal transport is likely to fluctuate as well. By altering the poleward mass and heat transport carried by the western boundary currents, the eddy-induced transport fluctuations can contribute substantially to regional and basin-scale climate variability (22–24).

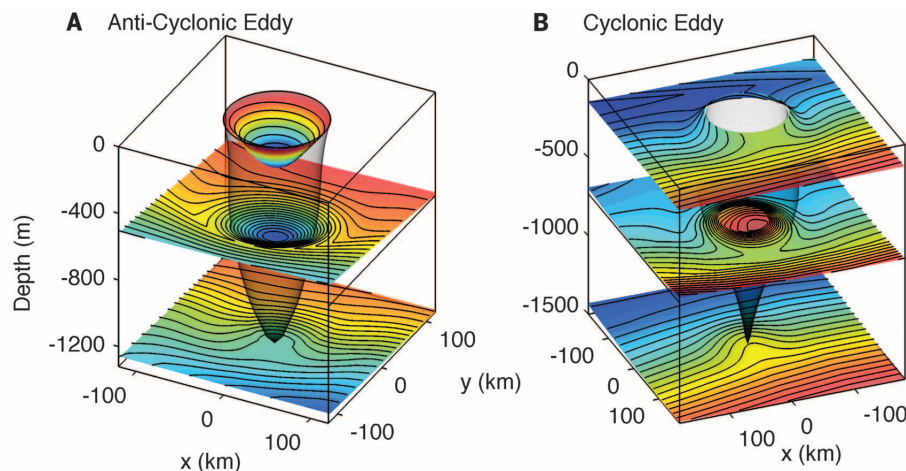


Fig. 2. 3D structures of trapped fluid by mesoscale eddies and PV distributions on representative isopycnals. (A) PV contours on three isopycnal surfaces of a warm-core eddy identified by the altimetry data at 30.1°N , 150.1°E in the subtropical North Pacific on 25 May 2005. The sea-level anomaly at the eddy center is 12 cm. The shape and depth of isopycnals are represented by the 3D surfaces. The potential densities of the upper, middle, and lower isopycnals are 23.35 kg m^{-3} , 26.59 kg m^{-3} , and 27.48 kg m^{-3} , respectively. PV distribution on the isopycnal is depicted by colored contours. The transparent black surface, defined by the outermost closed PV contours, signifies the boundary of fluid trapped by this warm-core eddy. (B) Same as (A) except for a cold-core eddy identified by the altimetry data at 30.7°N , 151.0°E in the subtropical North Pacific on 25 May 2005. The sea-level anomaly at the eddy center is -14 cm. The depicted isopycnal surfaces are 23.99 kg m^{-3} , 26.75 kg m^{-3} , and 27.56 kg m^{-3} , respectively.

Fig. 3. Global distribution of the zonal transport of fluid trapped by mesoscale eddies. (A) Eddy-induced zonal transport through meridional cross section per degree of latitude. The figure is based on the statistical average of eddy propagation speed and trapped fluid volume (15). (B) Distribution of the total meridionally integrated zonal transport induced by eddies as a function of longitude. The solid blue curve represents the westward transport and the solid red curve represents the eastward transport, computed by integrating the zonal transports in (A) from 80°S to 80°N. The dashed blue curve represents integrated total transport north of 40°S, and the dashed red curve represents integrated total transport south of 40°S.

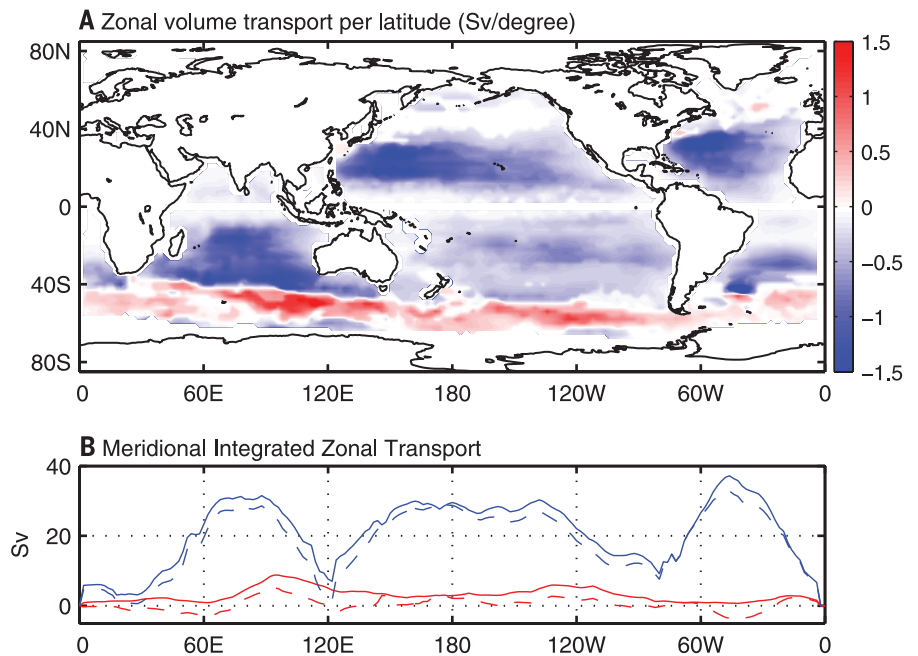
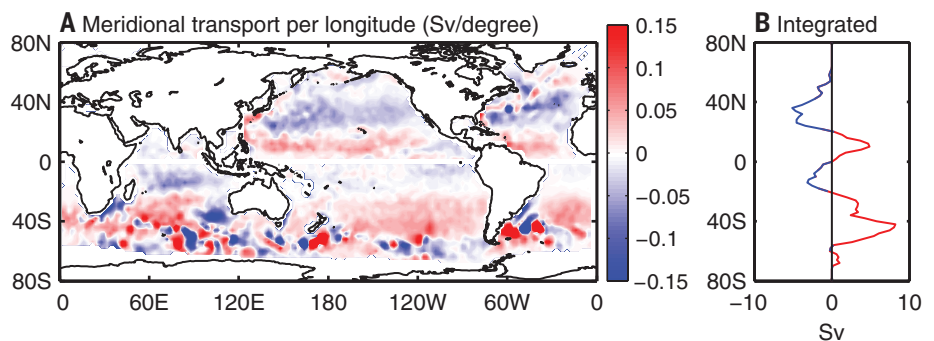


Fig. 4. Global distribution of the meridional transport of fluid trapped by mesoscale eddies. (A) Eddy-induced meridional transport through a zonal cross-section per degree of longitude. (B) Distribution of the total zonal-integrated meridional transport induced by eddies as a function of latitude.



It is worth noting that there exist no strong currents in many regions with large westward eddy-induced transport identified in Fig. 3A. Equally important, the eddy-induced transports can penetrate to the depth below the main thermocline, where the wind-driven circulation is generally weak. In these regions and depth ranges without strong background circulation, the mesoscale eddies can dominate the transport of heat, fresh water, and dissolved carbons and other biogeochemical tracers, which are important for understanding long-term climate change.

In climate models that simulate global warming scenarios, the transport by oceanic mesoscale eddies is generally underestimated and/or improperly resolved because of their coarse grid resolution. As the model resolution increases with enhanced computing power, mesoscale eddies will be progressively resolved by future climate models, and the impact of the eddy-induced transport will probably emerge. This makes the task of establishing proper theories about eddy-induced transport particularly important and urgent.

REFERENCES AND NOTES

1. G. Danabasoglu, J. C. McWilliams, P. R. Gent, *Science* **264**, 1123–1126 (1994).
2. S. Peacock, *Global Biogeochem. Cycles* **18**, GB2022 (2004).

3. H. L. Bryden, E. C. Brady, *J. Mar. Res.* **47**, 55–79 (1989).
4. D. B. Chelton, P. Gaube, M. G. Schlax, J. J. Early, R. M. Samelson, *Science* **334**, 328–332 (2011).
5. D. J. McGillicuddy Jr. et al., *Science* **316**, 1021–1026 (2007).
6. C. Dong, J. C. McWilliams, Y. Liu, D. Chen, *Nat. Commun.* **5**, 3294 (2014).
7. G. R. Flierl, *Geophys. Astrophys. Fluid Dyn.* **18**, 39–74 (1981).
8. J. J. Early, R. M. Samelson, D. B. Chelton, *J. Phys. Oceanogr.* **41**, 1535–1555 (2011).
9. M. M. Lee, D. P. Marshall, R. G. Williams, *J. Mar. Res.* **55**, 483–505 (1997).
10. F. J. Beron-Vera, Y. Wang, M. J. Olascoaga, G. J. Goni, G. Haller, *J. Phys. Oceanogr.* **43**, 1426–1438 (2013).
11. J. R. Luyten, J. Pedlosky, H. M. Stommel, *J. Phys. Oceanogr.* **13**, 292–309 (1983).
12. P. B. Rhines, W. R. Young, *J. Fluid Mech.* **122**, 347–367 (1982).
13. G. I. Taylor, *Proc. R. Soc. London A Contain. Pap. Math. Phys. Character.* **93**, 99–113 (1917).
14. Z. G. Zhang, Y. Zhang, W. Wang, R. X. Huang, *Geophys. Res. Lett.* **40**, 3677–3681 (2013).
15. Information on the observational data and analysis methods is available in the supplementary materials on Science Online.
16. D. B. Chelton, M. G. Schlax, R. M. Samelson, R. A. de Szoeke, *Geophys. Res. Lett.* **34**, L15606 (2007).
17. D. B. Chelton, M. G. Schlax, R. M. Samelson, *Prog. Oceanogr.* **91**, 167–216 (2011).
18. W. J. Schmitz Jr., *On the World Ocean Circulation: Volume I: Some Global Features/North Atlantic Circulation* (Technical Report WHOI-96-03, Woods Hole Oceanographic Institution, Woods Hole, MA, 1996).

19. W. J. Schmitz Jr., *On the World Ocean Circulation. Volume II: The Pacific and Indian Oceans/A Global Update* (Technical Report WHOI-96-08, Woods Hole Oceanographic Institution, Woods Hole, MA, 1996).
20. Y. L. Chang, L. Y. Oey, *Geophys. Res. Lett.* **38**, L08603 (2011).
21. B. Qiu, S. Chen, *J. Phys. Oceanogr.* **43**, 344–358 (2013).
22. S. Minobe, A. Kuwano-Yoshida, N. Komori, S. P. Xie, R. J. Small, *Nature* **452**, 206–209 (2008).
23. B. Qiu, *J. Phys. Oceanogr.* **30**, 1486–1502 (2000).
24. B. Qiu, *J. Phys. Oceanogr.* **33**, 2465–2482 (2003).
25. M. F. de Jong, A. S. Bower, H. H. Furey, *J. Phys. Oceanogr.* **44**, 427–444 (2014).

ACKNOWLEDGMENTS

We thank the reviewers for their constructive and detailed comments. This research was supported by the National Basic Research Priorities Program of China through grant 2013CB430303, the National Natural Science Foundation of China under grant 41276014, and the National Global Change Major Research Project of China through grant 2013CB956201. The sources of the data used in this paper are contained in the supplementary materials.

SUPPLEMENTARY MATERIALS

www.sciencemag.org/content/345/6194/322/suppl/DC1
Materials and Methods
Figs. S1 to S4
References

19 February 2014; accepted 16 June 2014
Published online 26 June 2014;
10.1126/science.1252418